XAFS study of local structure with picometer accuracy: Th_1 − xU_xO_2 and Th_1 − xPu_xO_2 solid solutions

J. Purans, G. Heisbourg, N. Dacheux, Ph. Moisy, S. Hubert

XAFS study of local structure with picometer accuracy: $Th_{1-x}U_xO_2$ and $Th_{1-x}Pu_xO_2$ solid solutions

J.Purans[1,2], G.Heisbourg[1], N.Dacheux[1], Ph.Moisy[3], S.Hubert[1]

[1] *Institut de Physique Nucléaire, Université Paris Sud, 91406- Orsay, France*

[2] *Dipartimento di Fisica dell'Università di Trento, 38050 Povo, Italy*

[3] *CEA- Marcoule- 30207 Bagnols/Cèze Cedex, France*

PACS:

61.10.Ht	X-ray absorption spectroscopy: EXAFS, NEXAFS, XANES, etc.
78.70.Dm	X-ray absorption spectra

Address for correspondence:

Prof. J.Purans[1]

Dipartimento di Fisica dell'Università di Trento

Via Sommarive 14

I-38050 Povo (Trento)

Italy

FAX: + 39-0461-88 16 80

E-mail: purans@science.unitn.it

*The paper submitted for publication in the Proceedings of the **XAFS-12** Conference.*

[1] E-mail: purans@science.unitn.it

Abstract

XAFS spectroscopy using synchrotron radiation is extremely suitable technique to study local atomic and electronic structure of mixed $Th_{1-x}U_xO_2$ and $Th_{1-x}Pu_xO_2$ oxides. Despite of XAFS technique overall success, the *pico-meter* barrier (10^{-2}Å) exists in an XAFS data analysis. Here we present the dependence of the mixed oxide structure on composition, probed by XAFS with *picometer accuracy*. Complimentary XAFS spectra were measured at the Th, U, and Pu L-edges. We found that opposite to the lattice parameter obtained by XRD, the distances given by XAFS for the first and second shells do not follow completely to neither the Vegard's law nor the virtual crystal approximation (VCA). The Th-O, U-O and Pu-O distances obtained vary slightly upon dilution. These values are close to the ones expected from the Vegard's law but are always smaller than the ones expected in VCA. The U-U(Th) and Th-Th(U) distances vary strongly upon dilution and the values are close to the ones expected from the VCA model but are always smaller than the ones expected by the Vegard's law. The average lattice parameter calculated from XAFS data agrees well with a random distribution of metal (Th, U, Pu) and with one calculated from XRD data. With this complementary XAFS data on the local structure around two selected metal ions it is then possible to give a better view on the mixed oxides structure, the distribution of the two metal ions and local distortions in such medium crystal structure studied by XRD.

1. Introduction

In the last decade, there has been a renewal of interest in studying the feasibility of thorium based fuel reactors as a potential advanced fuel for Generation IV nuclear energy systems that can be operated to relatively high burn-ups, and producing less minor actinides than uranium based fuel [1, 2]. Solid solutions of uranium and thorium oxide are being developed as fuel for the thermal breeding reactors and high temperature gas cooled reactors.

The lattice constant of $Th_{1-x}U_xO_2$ and $Th_{1-x}Pu_xO_2$ stoichiometric solid solutions changes linearly with x in the whole region, the feature commonly referred to as Vegard's law [3,4]. Such behaviour does not exclude a bimodal distribution of nearest-neighbour (NN) distances in the solid solutions as diffraction methods do not provide sufficient information on the local structure in disordered crystals [5]. It is somewhat surprising that the XAFS analysis well developed for solid solutions [6] has not yet been extensively exploited in the study of actinide dioxide solid solutions ($Th_{1-x}U_xO_2$, $U_{1-x}Pu_xO_2$, etc.).

2. Experimental details and data analysis

A series of solid solutions of $Th_{1-x}U_xO_2$ (x = 0.0, 0.11, 0.24, 0.37, 0.49, 0.65, 0.81, 0.91, 1) and $Th_{1-x}Pu_xO_2$ (x = 0.0, 0.13, 0.32, 0.66, 1.0) were prepared respectively in IPN (Orsay, France) and at CEA (Valhro, France) according the previously described procedure [2]. All the samples were characterized by using X-ray powder diffraction. The lattice constant of $Th_{1-x}U_xO_2$ and $Th_{1-x}Pu_xO_2$ solid solutions changes linearly with x in the whole region in a good agreement with the literature data [2-4].

The XAFS measurements of $Th_{1-x}U_xO_2$ and of $Pu_{1-x}U_xO_2$ solid solutions were performed on the D44 (XAS4) "hot" beam line of the LURE DCI synchrotron radiation facility (Orsay,

France). A standard transmission scheme with a Ge (400) double crystal monochromator and two ion chambers containing argon gas was used. The powders of $Th_{1-x}U_xO_2$ and of $Th_{1-x}Pu_xO_2$ solid solutions were finely ground and mechanically mixed with cellulose powder. The adjusted thickness of the samples permits us to reach a value for the absorption jumps between 0.2 to 0.8 depending on the composition of the solid solutions.

The XAFS were treated using the "EDA" software package following the standard procedure [6]. The experimental XAFS spectra $\chi(k)k^2$ were Fourier transformed (FT) with a Kaiser-Bessel window in the 0 - 15 $Å^{-1}$ range. In all the FT's of the experimental spectra (Fig. 1) there are two main peaks located at 1.9 Å and 3.8 Å with smaller pre peak at 3.2 Å, and lower peaks from 4.5 to 6 Å.

We have analysed the Th, U and Pu L_3-edge XAFS of the solid solutions to determine the change bond lengths in the first and second coordination shells as a function of solid solutions composition. Representative XAFS FT data for three different compositions are shown in Fig. 1 for the Th. As a general feature, the first peak in the Th, U and Pu FT of the solid solutions are sharp and show a small, but significant and gradual shift to those in the respective standards (ThO_2 and UO_2). The second peak is also sharp and more visible gradual shift from one end member to other.

The single-shell XAFS spectra were fitted using the single-scattering curved-wave formalism with picometer accuracy [8]. The XAFS data were analyzed using two different approaches: the phases and amplitudes were either calculated or obtained experimentally from a crystalline reference. Theoretical backscattering amplitudes and phases were calculated by the FEFF8 code using different clusters that mimic the possible environment of the An^{4+} ions in solid solutions, respectively [9].

3. Results and discussion

The interpretation of the XAFS spectra in $Th_{1-x}U_xO_2$ and $Th_{1-x}Pu_xO_2$ solid solutions is analogous to the pure oxides (see XAFS analysis of ThO_2, UO_2 and PuO_2 in ref. [10-13]) due to the very small differences in the scattering amplitude and phase shift functions of thorium, uranium and plutonium atoms: here the visible differences are only caused by the change of the lattice constant with the composition and by the very small differences in the scattering amplitude and phase shift functions of thorium and uranium (plutonium). The first effect is responsible for the shift in the energy position of the features of the FT while the second one for the small decrease of the second peak amplitude of the FT. We estimate that at room temperature the thermal broadening (Debye Waller factor) contributes $\sigma^2 = 0.005$ Å^2 to the DW factor in the Th-O and U-O near-neighbour distributions.

First-neighbor environment. From the XAFS fitting data in the first coordination shell we conclude that the R_{U-O}, R_{Th-O} and R_{Pu-O} distances vary linearly upon dilution in the solid solutions (Fig. 2 and 3). The values (R_{Th-O}, R_{U-O} and R_{Pu-O}) are closer to the ones expected from the Vegard's law (Pauling model - the partial molar volume of each constituent is independent of concentration) than to the ones expected from the VCA. We estimate an uncertainty of 0.003 Å in the near-neighbour distances, corresponding to a factor of 2 increase in the reliability of-fit parameter from a minimum value, expected in the dilute alloys (10 mol. %) where the error is ~0.005 Å. The total decrease in R_{Th-O} in $Th_{1-x}U_xO_2$ from pure ThO_2 to pure UO_2 (linear interpolation to 0 mol % Th in UO_2) is 0.019 ± 0.003 Å, or ~35% of the difference between R_{Th-O} and R_{U-O} in the end-point compounds (impurity limit). At the same time the increase in R_{U-O} from pure UO_2 to the impurity limit of U in ThO_2 is 0.026 ± 0.003 Å, or ~47% of the difference between R_{Th-O} and R_{U-O} in the end-point compounds. In comparison in the $Th_{1-x}Pu_xO_2$ from pure ThO_2 to pure PuO_2 (linear interpolation to 0 mol % Th in PuO_2) is 0.025 ± 0.003 Å, or ~32% of the difference between

R_{Th-O} and R_{Pu-O} in the end-point compounds that is in good agreement with the value (35%) obtained for the $Th_{1-x}U_xO_2$. So the local compressibility of [ThO_8] cluster is characteristic in these two solid solutions. At the same time the increase in R_{Pu-O} from pure PuO_2 to the impurity limit of Pu in ThO_2 is 0.0425 ± 0.005 Å, or ~54% of the difference between R_{Th-O} and R_{Pu-O} in the end-point compounds that is the highest "compressibility" observed.

Second-neighbour environment. On the contrary to the first shell, the U-U(Th) and Th-Th(U) distances vary strongly upon dilution (Fig. 4,5) and the values are close to the ones expected from the VCA model but are always smaller than the ones expected by the Vegard's law. We estimate an uncertainty of 0.005 Å in the second-neighbour distances, corresponding to a factor of 2 increase in the reliability-of-fit parameter from a minimum value, expected in the dilute alloys (10 mol.%) where the error is ~0.005 Å. The total decrease in $R_{Th-U(Th)}$ from pure ThO_2 to pure UO_2 (linear interpolation to 0 mol.% Th in UO_2) is 0.067 ± 0.003 Å, or ~71% of the difference between R_{Th-Th} and R_{U-U} in the end point compounds. At the same time the increase in $R_{U-Th(U)}$ from pure UO_2 to pure ThO_2 (linear interpolation to 0 mol % U in ThO_2) is 0.080 ± 0.003 Å, or ~86% of the difference between R_{Th-Th} and R_{U-U} in the end point compounds. The total decrease in $R_{Th-Pu(Th)}$ from pure ThO_2 to pure PuO_2 (linear interpolation to 0 mol.% Th in PuO_2) is 0.105 ± 0.010 Å, or ~84% of the difference between R_{Th-Th} and R_{Pu-Pu} in the end point compounds. At the same time the increase in $R_{Pu-Th(Pu)}$ from pure PuO_2 to pure ThO_2 is 0.105 ± 0.010 Å, or ~84% of the difference between R_{Th-Th} and R_{Pu-Pu} in the end point compounds.

4. References

1. J. Stephen Herring, P. E. MacDonald, K. D. Weaver, C. Kullberg, Nucl. Engineering and Design **203**, 65 (2001).

2. B. Fourest, T. Vincent, G. Lagarde, S. Hubert, P. Baudoin, J. Nucl. Mat. **282**, 180 (2000).
3. I. Cohen, R.M. Berman, J. Nucl. Mat **18**, 77 (1966); and K. Bakker, E.H.P. Cordfunke, R.J.M. Konings, R.P.C. Schram, J. Nucl. Mat. **250**, 1 (1997).
4. M.D. Freshley, H.M. Mattys, General Electric Report HW-76559, 11.6 (1962)
5. M.F.Trope, E.J.Garboczi, Phys.Rev.B **42**, 8405 (1990); Y.Cai and M.F.Trope, Phys.Rev.B **46**, 15872 (1992).
6. J.C. Mikkelsen, Jr. and J.B. Boyce, Phys. Rev. B **15**, 7130 (1983).
7. A. Kuzmin, Physica B **208&209**, 175 (1995); J. Physique IV (France) **7**, C2-213 (1997).
8. G. Dalba, P. Fornasini, R. Grisenti, J. Purans, Phys. Rev. Lett. **82**, 4240 (1999).
9. Rehr, J.J., Mustre de Leon, J., Zabinsky, S.I. and Albers, R.C., J. Am. Chem. Soc. **113**, 5135 (1991); Mustre de Leon, J., Rehr, J.J., Zabinsky, S.I. and Albers, R.C., Phys. Rev. B **44**, 4146 (1991).
10. N.T. Barrett, G.N.Greaves, B.T.M Willis, G.M. Antonini, and F.R. Thornley, J.Phys.C: Solid State Phys. **21**, L791 (1988).
11. Z. Wu and F. Farges, Physica B **266**, 282 (1999).
12. B.D.Begg, N.J.Hess, W.J.Weber, S.D.Conradson, M.J.Schweiger, R.C.Ewing, J. Nucl. Mat. **278**, 212 (2000).
13. M.K. Richmann, D.T. Redd, A.J. Kropf, S.B. Aase, M.L. Lewis, J. Nucl. Mat. **297**, 303 (2001).

LIST OF FIGURES

Figure 1: Fourier Transforms of the experimental XAFS $\chi(k)k^2$ (Th L_3-edge) of ThO_2, $Th_{0,51}U_{0,49}O_2$ and $Th_{0,21}U_{0,79}O_2$.

Figure 2: Variation of the interatomic distances Th-O (● upper line) and U-O (■ bottom line) with the composition $Th_{1-x}U_xO_2$. The variation of crystal lattice parameter (a/2) follows the Vegard's low (middle dotted line – XRD data). The average weighted distances (▲) calculated from the distances Th-O (●) and U-O (■) are shown.

Figure 3: Variation of the interatomic distances Th-O (■ upper line) and Pu-O (● bottom line) with the composition $Th_{1-x}Pu_xO_2$. The variation of crystal lattice parameter (a/2) follows the Vegard's low (middle solid line – XRD data). The average weighted distances (▲) calculated from the distances Th-O (■) and Pu-O (●) are shown.

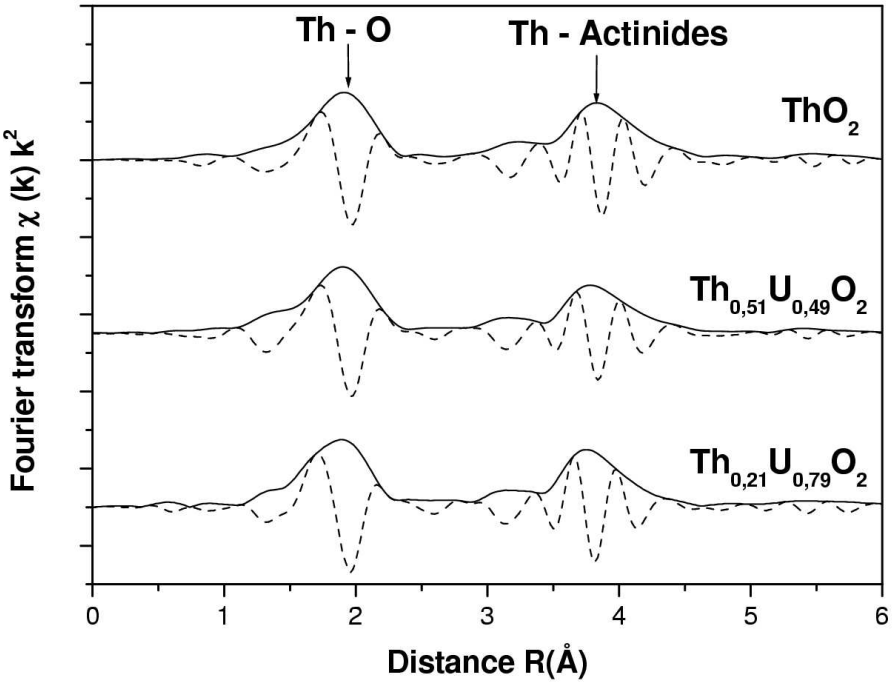

Fig. 1. Fourier Transforms of the experimental XAFS $\chi(k)k^2$ (Th L_3-edge) of ThO_2, $Th_{0,51}U_{0,49}O_2$ and $Th_{0,21}U_{0,79}O_2$.

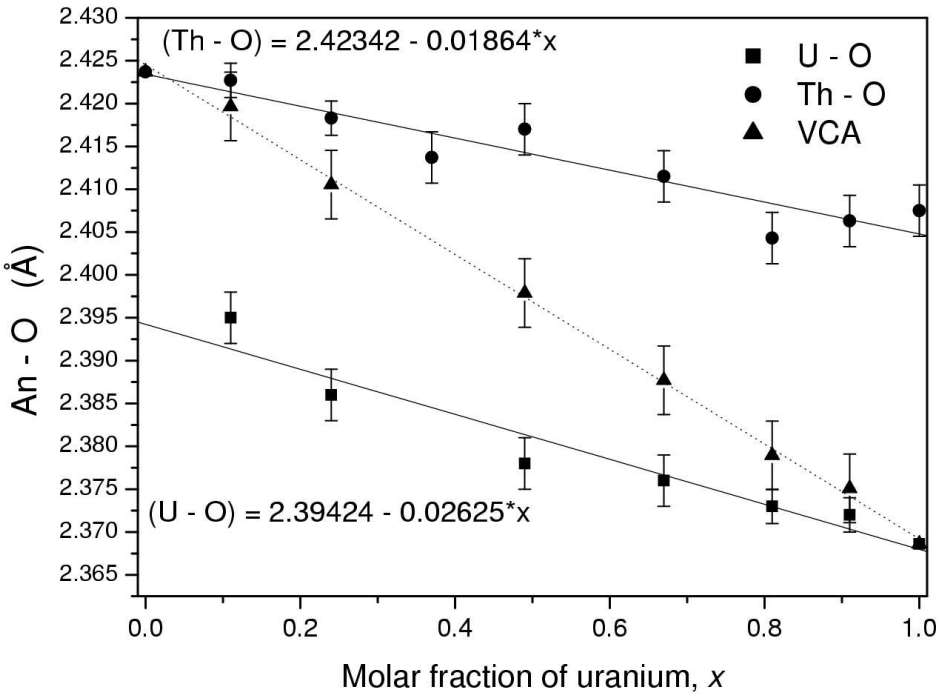

Fig. 2. Variation of the interatomic distances Th-O (● upper line) and U-O (■ bottom line) with the composition $Th_{1-x}U_xO_2$. The variation of crystal lattice parameter (a/2) follows the Vegard's low (middle dotted line – XRD data). The average weighted distances (▲) calculated from the distances Th-O (●) and U-O (■) are shown.

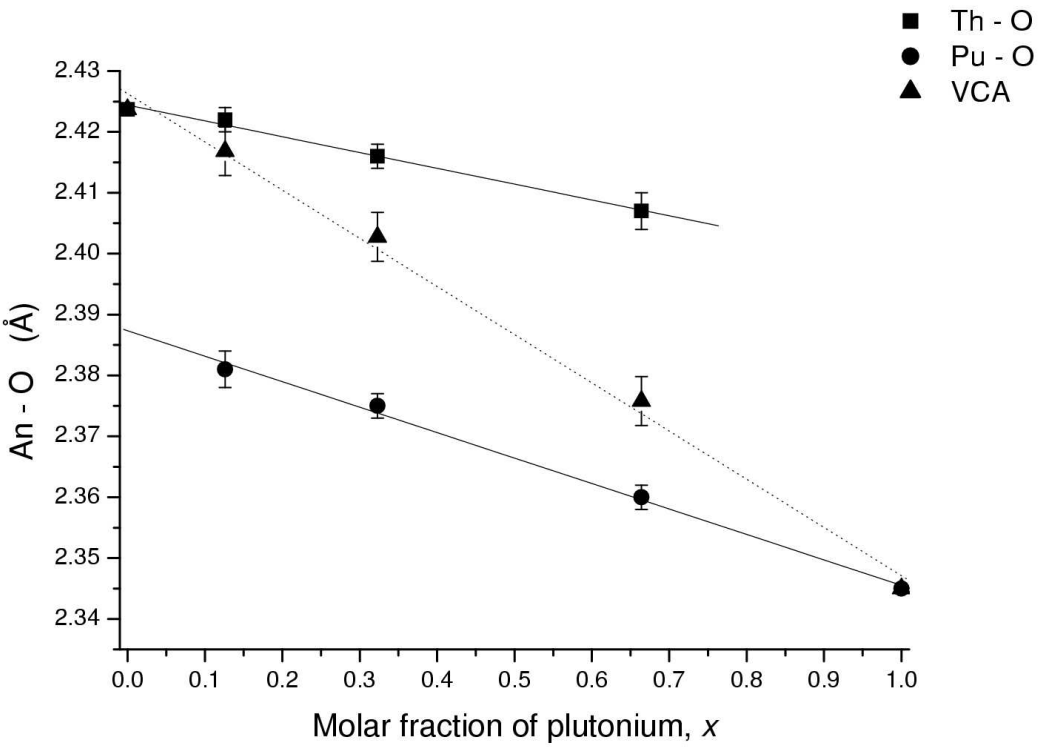

Fig. 3. Variation of the interatomic distances Th-O (■ upper line) and Pu-O (● bottom line) with the composition $Th_{1-x}Pu_xO_2$. The variation of crystal lattice parameter (a/2) follows the Vegard's low (middle solid line – XRD data). The average weighted distances (▲) calculated from the distances Th-O (■) and Pu-O (●) are shown.